

Spectroscopy of Seven Cataclysmic Variables with Periods Above Five Hours ¹

John R. Thorstensen and William H. Fenton

*Department of Physics and Astronomy
6127 Wilder Laboratory, Dartmouth College
Hanover, NH 03755-3528;
john.thorstensen@dartmouth.edu*

Cynthia J. Taylor

*The Lawrenceville School
P.O. Box 6008, Lawrenceville, NJ 08648*

ABSTRACT

We present spectroscopy of seven cataclysmic variable stars with orbital periods P_{orb} greater than 5 hours, all but one of which are known to be dwarf novae. Using radial velocity measurements we improve on previous orbital period determinations, or derive periods for the first time. The stars and their periods are TT Crt, 0.2683522(5) d; EZ Del, 0.2234(5) d; LL Lyr, 0.249069(4) d; UY Pup, 0.479269(7) d; RY Ser, 0.3009(4) d; CH UMa, 0.3431843(6) d; and SDSS J081321+452809, 0.2890(4) d. For each of the systems we detect the spectrum of the secondary star, estimate its spectral type, and derive a distance based on the surface brightness and Roche lobe constraints. In five systems we also measure the radial velocity curve of the secondary star, estimate orbital inclinations, and where possible estimate distances based on the $M_V(\text{max})$ - P_{orb} relation found by Warner. In concordance with previous studies, we find that all the secondary stars have, to varying degrees, cooler spectral types than would be expected if they were on the main sequence at the measured orbital period.

Subject headings: stars – individual; stars – binary; stars – variable.

1. Introduction

Cataclysmic variable stars (CVs) are close binaries in which a white dwarf accretes matter from a less evolved companion (the secondary), which usually resembles a lower-main-sequence

¹Based on observations obtained at the MDM Observatory, operated by Dartmouth College, Columbia University, Ohio State University, and the University of Michigan.

star. CVs have a rich phenomenology, and the theory of CVs involves contributions from many subdisciplines of astrophysics. Warner (1995) presents a comprehensive review.

Mass transfer in CVs occurs through Roche lobe overflow, so the secondary’s surface coincides almost exactly with the Roche lobe. This constrains the secondary’s mean density to be nearly fixed at a given orbital period P_{orb} . Because the mean density is a strong function of mass along the lower main sequence, there is a correlation between the secondary’s spectral type and the orbital period, with hotter, more conspicuous secondaries appearing at longer P_{orb} .

In many instances this simple picture is not accurate. As a cataclysmic evolves through mass transfer to shorter P_{orb} , the secondary star’s thermal timescale grows comparable to the orbital evolution time, leading to departures from thermal equilibrium and consequent discrepancies between reality and expectations based on main-sequence characteristics. Even so, Beuermann et al. (1998) found that the relatively small number of CV secondaries detectable in systems with $P_{\text{orb}} < 3$ h are fairly close to the main sequence, so these departures are evidently not severe in these cases. In contrast, a substantial fraction of *longer*-period secondaries are significantly cooler than expected; at any given P_{orb} , the hottest secondaries lie near the main sequence, but there are many cooler objects. This suggests that in many longer-period CVs, the secondaries have begun nuclear evolution prior to mass transfer (Baraffe & Kolb 2000). Further support for this scenario comes from Gänsicke et al. (2003), who point out anomalous nitrogen-to-carbon ratios in several CVs, indicating that the material being transferred has passed through CNO burning. Also, the anomalous objects EI Psc (= RX J2329+06) and QZ Ser have quite short periods (64 min and 2.0 hr respectively), yet show strong K-star features in their spectra; these secondaries are much too *early* for their orbital period. QZ Ser in addition shows enhanced sodium features which may indicate CNO-processed material (Thorstensen et al. 2002a,b). These anomalous systems are nicely matched by models in which mass transfer begins at longer periods after the onset of nuclear evolution. Their antecedents should be anomalously cool systems at longer periods.

Studies of longer-period systems can therefore provide useful empirical clues to CV evolution. Furthermore, when the secondary star’s contribution is visible, as it often is at longer periods, it offers practical advantages and opens several lines of investigation, as follows: (1) Because the secondary’s orbit is accurately circular, and its surface is free of significant non-orbital motion, the radial velocities of the secondary tend to be much better-behaved than emission line velocities, which can arise from complicated, variable flows of gas. It is easier to find P_{orb} from an accurately sinusoidal velocity curve than from the jittery velocities often found for emission lines. (2) Similarly, the secondary’s velocity curve should track its center-of-mass motion in a relatively accurate and straightforward manner. Complications can arise from nonuniformity of the secondary’s surface (especially asymmetries between the secondary’s front and back sides), but these are less severe than the gross difficulties often presented by emission lines. (3) If the emission-line velocities are to trace the white dwarf’s motion, it is necessary (but not sufficient) for their phase to be one-half cycle away from the secondary’s motion. In non-eclipsing CVs there is often no absolute marker of binary phase, but when secondary star radial velocities are measurable, they provide just such

a marker. If the emission and absorption phases differ by 180 degrees, as expected, it is at least *possible* that the emission lines follow the white dwarf motion; if so, a mass ratio can be computed. (4) The kinematics of the CV population provide a clue to their age and evolutionary status (Kolb & Stehle 1996). As North et al. (2002) point out, the secondary spectra can provide systemic radial velocities which are more reliable than those inferred from emission lines, provided the zero point is established carefully. (5) At a given orbital period, the Roche lobe constraint makes the secondary’s radius a weak function of its mass. An accurate spectral type for the secondary constrains its surface brightness, which together with the radius yields an estimate of the absolute magnitude. If the secondary’s contribution to the system’s light can be measured, this gives a distance estimate.

In this paper we present studies of seven longer-period systems. In all cases the P_{orb} is either determined for the first time or improved. We detect the secondary stars and, insofar as possible, perform the analyses outlined above. Section 2 outlines the methodology, Section 3 details results for the individual stars, and Section 4 is a brief discussion.

2. Techniques

Table 1 is a journal of our observations. We obtained spectra at the MDM Observatory at Kitt Peak, Arizona, mostly with the 2.4m Hiltner telescope, with a few observations from the 1.3m McGraw-Hill telescope. At the 2.4m we used the ‘modular’ spectrograph, a 600 line mm^{-1} grating, and a SITe 2048² CCD detector yielding 2 Å pixel^{-1} from 4210 to 7560 Å (vignetting severely toward the ends), and typical resolution of 3.5 Å FWHM; at the 1.3m, we used the Mark III spectrograph and a 1024² SITe CCD giving 2.2 Å pixel^{-1} from 4480 to 6780 Å, with 4 Å FWHM resolution. A 1-arcsec slit was used at the 2.4 m, and a 2-arcsec slit at the 1.3 m. In order to maintain an accurate wavelength calibration we took exposures of comparison lamps hourly as the telescope tracked, and whenever the telescope was moved. The measured wavelength of the $\lambda 5577$ night-sky line provided a check; it was generally stable to less than 10 km s^{-1} in the reduced spectra. For a few of the 1.3m spectra we were unable to take comparison lamps because of equipment trouble, and we calibrated these by using the night sky lines to find a zero-point offset for each spectrum.

When the sky was suitably clear, we took spectra of flux standards to derive the instrument response function. We also observed bright B stars and used these spectra to derive an approximate correction for telluric absorption bands. For most of our 2.4 m observations, we rotated the spectrograph slit to the parallactic angle to avoid dispersion losses. Even so, our individual 2.4 m data often showed unphysical, irreproducible fluctuations in the continuum shape, which we still do not understand; however, these appear to average out over many exposures. Such averaging occurs both in the computation of the instrument response function and the compilation of our mean program-object spectra, so the continua in our mean spectra should be reasonably accurate.

For our reductions we used standard IRAF² procedures for flatfielding, extraction of one-dimensional spectra, wavelength calibration, and flux calibration.

Our main goal was to determine orbital periods for these systems from radial velocities. To measure emission line velocities (almost exclusively H α) we used tunable convolution algorithms described by Schneider & Young (1980). We also computed a velocity error estimate by propagating the counting-statistics errors generated by the IRAF reductions. In most cases the scatter of the data around the best-fitting sinusoid significantly exceeded the counting-statistics estimates, indicating that the emission line profiles were not particularly well-behaved.

In some cases we tried to extract dynamical information from the emission lines using the technique pioneered by Shafter (1983) (hereafter the ‘Shafter diagram’ technique). In this, one convolves the emission line with an antisymmetric function consisting of a positive and a negative Gaussian with a tunable separation α , and repeats the measurement and sinusoidal fit with increasing separations until the velocity errors become excessive. The sinusoid fitted to the velocities measured with the widest separation at which the errors are reasonable is taken to represent the motion of the white dwarf. This procedure measures the high-velocity wings of the line, which are produced close to the white dwarf, where one hopes that the rapid rotation of the disk smooths out asymmetries. There are many cataclysmics in which this hope is clearly not realized; when an absolute phase marker is available (such as an eclipse), the phase of the emission-line velocities in some systems does not track the known phase of the white dwarf’s motion. In most of the stars studied here we do have an absolute phase marker – the secondary star’s velocity curve (see below) – so the emission-line phases can be checked to see if they at least agree with expectation. Such agreement is a necessary, but not sufficient, condition for the emission velocities to be dynamically faithful. We use them, but caution the reader that they may not be quite right.

None of the systems studied here are known to eclipse, so their inclinations are not known with enough precision to find accurate masses. However, as noted earlier the absorption-line radial velocities give a relatively straightforward measure of the secondary’s projected orbital velocity, and this can be used to establish constraints on the orbital inclination, provided the masses are within realistic limits. Warner (1987) found a relationship in dwarf novae between P_{orb} and the inclination-corrected absolute magnitude at maximum light, $M_V(\text{max})$. In several cases here our dynamically-constrained inclinations are accurate enough to use this relationship to estimate distances.

K-type secondaries were evident in several of these objects. For these we measured absorption-line velocities using the *xcsao* cross-correlation radial velocity package (Kurtz & Mink 1998). We mostly correlated the range from 5050 to 6500 Å, excluding the complicated region around NaD (which usually included HeI λ 5876 emission); for some objects restricted the correlation to the 6000 to 6500 Å region. The *xcsao* task produces an error estimate based on the *R*-statistic developed by Tonry & Davis (1979); in well-exposed spectra the estimated uncertainty was often $\lesssim 10$ km

²IRAF is distributed by the National Optical Astronomy Observatories.

s^{-1} . The scatter of the velocities around the best sinusoidal fits was generally comparable to the Tonry-Davis errors, indicating that they are fairly realistic.

For the cross-correlation template spectrum, we used a velocity-compensated sum of 86 observations of IAU velocity standards, accumulated over the past several years with the same equipment and procedures used for the program objects. The standards were all K or late G stars, mostly giants. When the individual velocity standard spectra were cross-correlated against this sum, the RMS scatter of the observations around the cataloged velocities was 7.1 km s^{-1} . The photon statistics of the standard star observations were always excellent, so this test is dominated by systematic effects, including (1) spectral mismatch of the individual stars compared to the sum, (2) imperfections in the wavelength calibration, and (3) mis-centering of the star in the spectrograph slit, leading to spurious wavelength shifts. Because of the large number of standard observations, we estimate that the zero point is determined to $\sim 2 \text{ km s}^{-1}$. The stars below typically have dozens of observations, so the formal errors on their γ (i.e., mean systemic) velocities are often very small, but we estimate the external accuracies of γ to be $\sim 5 \text{ km s}^{-1}$; spectral mismatches, subtle asymmetries in the surfaces of the CV secondaries, and other imponderables probably enter around this level.

For period searches, we used a ‘residual-gram’ technique described in Thorstensen et al. (1996). This works especially well for data which follow a sinusoid accurately. Because the time sampling was nonuniform, numerous alias periods typically turn up in the period searches, corresponding to differences in the cycle count during gaps in the data. These manifest as candidate frequencies separated by $1/T$, where T is the length of the gap; $T = 1 \text{ d}$, for example, corresponds to the daily cycle count ambiguity. In some of the objects the choice of alias was clearly unambiguous, but where needed we applied the Monte Carlo procedure described by Thorstensen & Freed (1985) to determine the confidence with which the best-fitting period could be identified with P_{orb} . Once a period was adopted, the variation was fitted with sinusoids

$$v(t) = \gamma + K \sin[2\pi(t - T_0)/P]$$

using a hybrid linear least-squares algorithm. Note that T_0 is the epoch of apparent inferior conjunction of the source being observed. If the source is the secondary, T_0 is the epoch at which eclipses of the white dwarf would be expected if the system were edge-on.

To characterize the secondary’s spectral contribution, we began by shifting the individual spectra into the rest frame of the secondary spectrum, using the fitted sinusoidal orbit and the *rvsao* task *sumspec*, and then averaged these. We have a set of spectra of K-dwarfs classified by Keenan & McNeil (1989), observed with our standard 2.4 m instrumentation, and a similar set of M-dwarf spectra classified by Boeshaar (1976). We shifted these to zero velocity, scaled each spectrum using a range of multiplicative factors, and subtracted the scaled spectra from the program object’s velocity-compensated spectrum. Finally, we examined all these subtracted spectra by eye and decided on a range of acceptable spectral types and flux contributions for the secondary, based on how well the secondary’s spectral features had been removed from the original spectrum.

Tables in Beuermann et al. (1999) can be used to find surface brightnesses as a function of spectral type, and expressions in Beuermann et al. (1998) yield an estimated size of the secondary star given the orbital period and an estimate of the secondary’s mass. The secondary mass is generally unknown, but the radius depends only on its cube root; as a guide, we use the evolutionary calculations of Baraffe & Kolb (2000) to estimate a range of plausible secondary masses at the system’s P_{orb} and secondary spectral type. The surface brightness, radius, and flux then yield a distance estimate. Note that this procedure does *not* assume that the absolute magnitude of the secondary is appropriate to its spectral type on the main sequence, but only that the secondary’s *surface brightness* is appropriate to its spectral type.

To compute the magnitude of the secondary star alone, we applied the IRAF *sbands* task to the subtracted K-star spectrum. This task synthesizes magnitudes from a flux-calibrated spectrum using a passband, in this case the V passband tabulated by Bessell (1990). To check this procedure we synthesized V magnitudes for the flux standard stars and the bright B stars used to map the continuum and band shapes. Over several observing runs the rms variation of the synthetic-minus-catalog magnitudes for these stars was 0.15 mag, with mean zero-point offsets of less than 0.1 mag. These stars may have been centered in the slit a little more attentively for these brief exposures than for the longer sequences on the program stars, and conditions may have been better on average so we adopt 0.25 mag as the contribution of the calibration to the error budget. Because standard star observations were only taken when the sky appeared clear, but program star observations were taken whenever possible, we assume that our secondary stars are ~ 0.2 mag brighter than our calibrations would indicate.

Several of these systems are substantially reddened. For all of the distance calculations, we used the Schlegel, Finkbeiner, & Davis (1998) maps to estimate the reddening, sometimes reducing the implied A_V if it appeared likely that the star did not lie entirely outside the Galaxy’s dust layer. In most cases the uncertainty in the reddening contributed little to the error budget.

3. The Individual Stars

The results for all the stars are summarized in tables and figures. Table 2 gives parameters of the emission lines measured from the mean fluxed spectra; in many cases the NaD absorption lines, blended at this resolution, are included as well. Table 3 lists all the radial velocities. Table 4 gives parameters of sinusoidal fits to the velocities, and Table 5 gives derived characteristics of the secondary stars and summarizes a secondary-based distance estimate for each system. Fig. 1 shows the mean fluxed spectra of all the objects, and Fig. 2 shows the folded radial velocity curves.

3.1. TT Crt

Szkody et al. (1992) obtained spectroscopy and photometry of this system and found candidate orbital periods of 438 and 445 min. They detected the secondary star in the spectrum, and estimated a spectral type of K5 - M0. Time-series photometry showed apparent ellipsoidal variations.

Our observations of TT Crt span 1262 d. The absorption velocities follow a sinusoid with large amplitude and little scatter, and the cycle count over the whole interval is determined without ambiguity, yielding $P_{\text{orb}} = 0.268351(1)$ d, or 386 min. The H α emission velocities, while less accurate, independently constrain the period to the same value within the uncertainties. Although the candidate periods found by Szkody et al. (1992) are similar to the more reliable period found here, they are formally inconsistent with the present result and appear to reflect a mistaken cycle count over a 2-day interval. Szkody et al. (1992) do give an epoch of apparent inferior conjunction of the secondary star in 1991 February, and our period is precise enough to extrapolate back to their observation without ambiguity, yielding a refined ephemeris,

$$\text{Secondary inferior conjunction} = \text{HJD } 2,452,297.025(1) + 0.2683522(5)E,$$

where E is an integer.

The flux-decomposition procedure yielded $K5 \pm 1$, toward the early end of the range found by Szkody et al. (1992). As Szkody et al. (1992) pointed out, the emission lines in TT Crt are double-peaked most of the time; H-alpha shows a separation of ~ 670 km s $^{-1}$.

TT Crt has the largest absorption-line velocity amplitude K_{abs} of the systems studied here. The Shafter diagram showed the emission lines to be accurately antiphased to the absorption, and to have a velocity amplitude K_{eml} fairly insensitive to the convolution function width α ; we adopted $\alpha = 1800$ km s $^{-1}$ for the emission-line measurements, which yields a nominal $q = M_2/M_1 = 0.58$. Curiously, the fits show the emission line mean velocity γ_{em} to be a function of α , and γ_{em} disagrees significantly with the corresponding value for the absorption lines γ_{abs} . For the reasons noted earlier we believe γ_{abs} to be the more reliable measure of the systemic velocity. The photometry presented by Szkody et al. (1992) is extensive enough to rule out any significant eclipse, which constrains the inclination i to be less than about 70 degrees to avoid an obvious partial eclipse of the disk. At $i = 70$ degrees the minimum white dwarf mass is around $0.8 M_{\odot}$. A comfortable fit to all the data occurs for $M_1 = 1.0 M_{\odot}$ and $i = 60$ degrees. The inferred white dwarf mass exceeds the Chandrasekhar limit for $i \lesssim 52$ degrees. As always, these constraints could be relaxed slightly if the measured K_2 misrepresents the secondary's center-of-mass motion, but the inclination is rather tightly constrained, and it is unlikely that the M_1 is less than $0.7 M_{\odot}$. Also, the estimate of the secondary's mass used to estimate the Roche lobe size in the distance calculation, $M_2 = 0.5 - 0.8 M_{\odot}$, is consistent with the mass ratio only if the white dwarf is $\sim 1 M_{\odot}$. While there is no guarantee that our adopted secondary mass is correct, the distance estimate fortunately depends only weakly on the assumed M_2 .

At $i = 60 \pm 10$ degrees, the Warner (1987) M_V - P_{orb} relation predicts $M_V = 4.1 \pm 0.5$, where

the uncertainty shown is purely from the uncertainty in the inclination. The General Catalog of Variable Stars (GCVS; Kholopov et al. 1999) gives $V_{\max} = 12.5$, and the extinction is about 0.1 mag, yielding $(m - M)_0 = 8.3$ mag, or 460 pc. The estimate based on the secondary is 9.4 mag, or 760 pc. These are broadly in agreement, but a little more discrepant than might be expected.

3.2. EZ Del

EZ Del was misidentified in the Downes & Shara (1993) atlas. Liu, Hu, Zhu, & Li (1999) found that a star 7 arcsec SE of the marked star showed a typical CV spectrum, and the correct star is marked in Downes et al. (2001).

The 2002 June velocities are best fit by a frequency near 5.5 cycle d^{-1} , while the 2003 June velocities indicate 4.5 cycle d^{-1} . The 2003 June observations were timed to improve discrimination of the cycle-count aliases, and the 4.5 cycle d^{-1} gives the better fit to the combined data, which has a discriminatory power (defined by Thorstensen & Freed 1985) near 0.98. The daily cycle count is therefore fairly clear but not absolutely secure. The period listed in Table 4 is the weighted average of periods found in separate fits to the two observing runs; the (unlikely) alternate daily cycle count would give $P_{\text{orb}} = 0.1822(5)$ d. An unknown of cycles elapsed in 1-year gap between observations, leaving the precise period ambiguous. Allowed periods lying within ± 4 standard deviations of the period in Table 4 are given by $P = 373.830(3)\text{d}/N$, where the integer $N = 1673 \pm 15$.

The mean fluxed spectrum of EZ Del is quite blue, and the mean spectra from 2002 June and 2003 June differ significantly. The 2002 June spectrum had a synthetic V magnitude of 17.6, and a 4500 to 7500 Å continuum fit well by $f_{\lambda} \propto \lambda^{-1.76}$, while the 2003 June spectrum had 18.0 and a power-law exponent of -0.92 , still rather bluer than most dwarf nova at minimum light. It thus appears that neither of our spectra were taken fully at minimum. Exploratory spectra taken 1999 June 10.4 UT and 2001 June 24.3 UT both showed the star in outburst, with synthetic V magnitudes of 15.3 and 15.7 respectively; these limited observations suggest that EZ Del outbursts frequently.

A late-type secondary star is detected in the spectrum, but because of the modest signal-to-noise and the secondary’s small fractional contribution, it is subtle; only the broad TiO bands are visible at low amplitude. We could not measure radial velocities of the secondary star, and with no absolute phase marker we choose not to infer dynamical information from the emission line velocities.

3.3. LL Lyr

Smith, Sarna, Catalan, & Jones (1997) detected the TiO bands and Na $\lambda 8190$ doublet of the secondary star. Our summed, fluxed spectrum shows clear features of an M-dwarf secondary

and relatively broad emission lines whose peaks are not quite doubled. The system’s synthetic V magnitude is 17.8.

The emission-line velocities of LL Lyr are from six observing runs spanning 1083 d, and define an unambiguous cycle count over the entire interval, yielding $P_{\text{orb}} = 0.249069(5)$ d. While the signal-to-noise ratio of the secondary star’s spectrum was inadequate for velocity measurements, we could again estimate the secondary contribution and infer a distance. Our spectral type estimate, $M2.5 \pm 1.5$, is in satisfactory agreement with the M3 - M4 classification found by Smith, Sarna, Catalan, & Jones (1997). LL Lyr is an example of a long-period dwarf nova with a secondary which is considerably later than would be expected for the main sequence.

Again, without velocities of the secondary, we do not attempt a dynamical analysis.

3.4. UY Pup

Lockley et al. (1999) obtained spectra in outburst and estimated $P_{\text{orb}} = 10.22 \pm 0.19$ h. They inferred a low orbital inclination.

UY Pup outbursts frequently, and the mean spectrum shows a blue continuum and a relatively weak secondary contribution despite the long orbital period. Our mean spectrum evidently was taken when the system was above minimum light.

The time series spans 603 days, and we find consistent, unambiguous periods in both the emission and absorption lines, the weighted mean being $0.479269(7)$ d, or 11.50 h. Thus the previous period is again similar to, but formally inconsistent with, the more accurate period found here. The secondary star, for which we find K2 - K6, is clearly not on the main sequence, since a main sequence secondary in this period regime would be much earlier (Lockley et al. 1999).

Because K_2 is fairly small at 102 ± 4 km s⁻¹, the inclination is low and is confined to a rather narrow range. The Shafter diagram shows K_{em} increasing with the convolution width α . If we adopt $\alpha = 1200$ km s⁻¹, then $K_{\text{em}} = 96$ km s⁻¹, and the mass ratio $q = M_2/M_1$ is fairly close to unity, but the sensitivity of K to α suggests that this is not particularly reliable. A $0.8 M_{\odot}$ white dwarf and $0.6 M_{\odot}$ secondary at $i \sim 40$ degrees fits all the data nicely. If we demand that $q < 1$, and that $M_1 > 0.5$ solar masses, then $i < 50$ degrees; keeping the white dwarf mass well below the Chandrasekhar limit requires $i > 25$ degrees.

Adopting $i = 38$ degrees, the Warner (1987) relation yields $M_V(\text{max}) = 2.3$, and because the inclination correction flattens out toward low inclination the resulting uncertainties are small. The GCVS gives the photographic magnitude at maximum as 13.0. Since dwarf novae in outburst have small color indices, we take this as V_{max} and assume $A_V = 0.5$ to find $(m - M)_0 = 10.2$, or $d = 1100$ pc. This agrees very well with the estimate from the secondary star (Table 5).

3.5. RY Ser

This dwarf nova was mis-identified in the Downes, Webbink, & Shara (1997) atlas, but is correct in the on-line *Living Edition* of the atlas (Downes et al. 2001). Perhaps because of its historically uncertain identification, relatively little information is published.

The mean flux-calibrated spectrum implies $V \sim 16.4$, relatively bright for an unstudied dwarf nova. The secondary star is clearly detected. The emission lines are relatively narrow and single-peaked.

Although our observations of this system are sparse (only 14 exposures in a single run), both the secondary star’s velocities and the $H\alpha$ emission velocities unambiguously indicate a period near 0.30 days, the weighted mean being 0.3009(4) d. Because K_{abs} is small at $87 \pm 6 \text{ km s}^{-1}$, the inclination must be quite low. From the Shafter diagram we adopted $\alpha = 1060 \text{ km s}^{-1}$, yielding $K_{\text{em}} = 73 \pm 10 \text{ km s}^{-1}$, implying $q \sim 0.8$. Demanding $M_1 > 0.5$ constrains i to be less than about 31 degrees. A good fit is obtained at $M_1 = 0.8 M_{\odot}$, $M_2 = 0.6 M_{\odot}$, and $i = 26$ degrees.

The Warner (1987) relation predicts $M_V(\text{max}) = +3.1$ with little uncertainty introduced by the inclination. For $V_{\text{max}} = 13.1$ (Mattei 2003), and a very substantial $A_V = 1.2$, this gives $(m - M)_0 = 8.8$, or 580 pc. The secondary star gives a distance in close agreement.

3.6. CH UMa

Thorstensen (1986) found an 8.3-hour radial velocity period in the Balmer lines in CH UMa, but could not exclude a 12.5-hour daily alias. Friend et al. (1990) obtained radial velocities of the secondary by cross-correlation near the 8190 Å Na doublet, and confirmed the 8.3-hour alias choice. They also found a statistically significant orbital eccentricity $e = 0.10$, which is unexpected in a CV, the orbits of which are expected to circularize quickly.

The mean fluxed spectrum shows a strong secondary contribution and quite narrow emission lines. The synthetic magnitude is $V = 15.2$.

Because of the brightness and the strong secondary contribution, the 28 cross-correlation velocities of CH UMa are relatively precise, with mean Tonry-Davis errors near 10 km s^{-1} and an rms scatter about the best sinusoidal fit near 8 km s^{-1} . Our data span 1259 d and, taken alone, constrain the period to 0.343181(4) d, with no ambiguity in cycle count. Friend et al. (1990) give an epoch of red-to-blue crossing of the absorption velocity, which can be connected to our fits without ambiguity, yielding the ephemeris

$$\text{Secondary inferior conjunction} = \text{HJD } 2,452,442.788(3) + 0.3431843(6)E,$$

where E is an integer.

We see no indication of the eccentricity in the secondary-star orbit noted by Friend et al.

(1990). The residuals as a function of phase showed no trends suggesting eccentricity. Fitting the velocities with an eccentric orbit yielded a best-fit $e = 0.012$, insignificantly different from zero, and the fit improved only marginally. Fixing the eccentricity held at their best-fit $e = 0.10$ led to slightly worse fits than with a circular orbits. We have somewhat fewer measurements than Friend et al. (1990) (28 to their 38), but our accuracy appears to be comparable, so the non-confirmation has some weight; we cannot rule out a nonzero eccentricity but we regard it as somewhat unlikely. A definitive test would require more phase coverage and better radial-velocity accuracy. Our fitted velocity amplitude $K = 76 \pm 3$ agrees well with that measured by Friend et al. (1990) (78 ± 3), but our mean velocity γ disagrees slightly (-15 ± 2 against their -3 ± 3).

3.7. SDSS J081321+452809

This object (hereafter SDSS0813) is one of the substantial number of CVs turned up by the Sloan Digital Sky Survey. Szkody et al. (2002) presented a spectrum, noted the presence of a late-type companion, and suggested that the orbital period was likely to be fairly long.

Our mean fluxed spectrum closely resembles that found by Szkody et al. (2002), with relatively narrow emission lines and a strong secondary spectrum. The synthetic $V = 18.4$ is similar to the $g^* = 18.29$ measured in the Sloan survey (Szkody et al. 2002).

We have 26 spectra; $H\alpha$ emission was measurable in all of them, and usable absorption velocities were found for all but three. A single spectrum was obtained 2002 Feb. 19, and the remainder were obtained on another observing run 30 days earlier. When the Feb. 19 point is omitted, the remaining emission and absorption velocities give similar periods, with no daily cycle count ambiguity; their weighted average is 0.289(1) d. The Feb. 19 point introduces cycle count ambiguity across the 30-day gap, the most likely choice yielding 0.2890(4) with 0.2867(4) d being somewhat less favored. Szkody et al.’s suggestion of a long period is evidently correct.

The distance based on the secondary star is around 2.1 kpc, which at the rather high Galactic latitude (32.9 deg) puts the system over 1 kpc from the Galactic plane. The distance uncertainty quoted in Table 5 is a quadrature sum of the various uncertainties. To establish a smallest plausible distance, we skew all the contributing quantities in the sense minimizing the distance, and find 1500 pc, which still puts the system 800 pc from the plane.

This system is notable as a long orbital period CV which is not known to erupt. If it were to undergo dwarf nova eruptions, the Warner (1987) relation predicts it would reach $V = 14.7$ at its inclination and distance. It is conceivable that eruptions of this magnitude could have been overlooked, so a dwarf-nova classification remains a possibility.

4. Discussion

As noted earlier, the secondaries in long-period cataclysmics are mostly later than expected on the basis of main-sequence models, with the edge of the observed distribution coinciding approximately with main-sequence expectations (Beuermann et al. 1998 and Baraffe & Kolb 2000 plot known systems on the spectral-type vs. P_{orb} diagram). The present small sample is nicely consistent with previous results. TT Crt comes the closest to the main-sequence spectral type expected for its period, missing it by only two subclasses, while UY Pup, CH UMa, and LL Lyr are all far cooler than predicted by main-sequence models. UY Pup is also notable for its unusually long period.

Because we detect and classify the secondary stars in all these systems, we can find distances based on the secondaries' surface brightnesses. For the four dwarf novae in which the secondary velocity curve allows us to also estimate the inclination, we derive an alternate distance estimate using the Warner (1987) $M_V(\text{max})$ - P_{orb} relation. Reasonably good agreement is found.

We confirm the conjecture by Szkody et al. (2002) that SDSS0813 is a long-period system; the inferred distance is therefore large, and SDSS0813 lies far from the Galactic plane. Dwarf nova eruptions, if present, have been overlooked. Tappert et al. (2001) discuss another long-period system at high latitude, CW 1045+525, which is also not known to outburst. Like SDSS0813, CW 1045+525 was not discovered through its variability, but rather in the Case objective-prism survey. The SDSS, which selects peculiar objects through accurate color photometry and follows them up with spectroscopy, may finally provide the basis for an accurate accounting of the CV population.

Acknowledgments. The NSF supported this work through grants AST 9987334 and AST 0307413. We thank the MDM staff for supporting the many observing runs on which these data were taken.

REFERENCES

- Baraffe, I., Kolb, U. 2000, MNRAS, 318, 354
- Bessell, M. S. 1990, PASP, 102, 1181
- Beuermann, K., Baraffe, I., Kolb, U., & Weichhold, M. 1998, A&A, 339, 518
- Beuermann, K., Baraffe, I., & Hauschildt, P. 1999, A&A, 348, 524
- Boeshaar, P. 1976, Ph. D. thesis, Ohio State University
- Downes, R. A. & Shara, M. M. 1993, PASP, 105, 127
- Downes, R., Webbink, R. F., & Shara, M. M. 1997, PASP, 109, 345
- Downes, R. A., Webbink, R. F., Shara, M. M., Ritter, H., Kolb, U., & Duerbeck, H. W. 2001, PASP, 113, 764
- Friend, M. T., Martin, J. S., Connon-Smith, R., & Jones, D. H. P. 1990, MNRAS, 246, 654
- Gänsicke, B. T. et al. 2003, ApJ, 594, 443
- Keenan, P. C., & McNeil, R. C. 1989, ApJS, 71, 245
- Kholopov, P. N. et al. 1999, VizieR Online Data Catalog, 2214,
- Kolb, U. & Stehle, R. 1996, MNRAS, 282, 1454
- Kurtz, M. J. & Mink, D. J. 1998, PASP, 110, 934
- Liu, W., Hu, J. Y., Zhu, X. H., & Li, Z. Y. 1999, ApJS, 122, 243
- Lockley, J. J., Wood, J. H., Jones, D. H. P., & Mineshige, S. 1999, Ap&SS, 266, 453
- Mattei, J. A. 2003, Observations from the AAVSO International Database, private communication.
- North, R. C., Marsh, T. R., Kolb, U., Dhillon, V. S., & Moran, C. K. J. 2002, MNRAS, 337, 1215
- Schlegel, D. J., Finkbeiner, D. P., & Davis, M. 1998, ApJ, 500, 525
- Schneider, D. and Young, P. 1980, ApJ, 238, 946
- Shafter, A. W. 1983, ApJ, 267, 222
- Smith, R. C., Sarna, M. J., Catalan, M. S., & Jones, D. H. P. 1997, MNRAS, 287, 271
- Szkody, P., Williams, R. E., Margon, B., Howell, S. B., & Mateo, M. 1992, ApJ, 387, 357
- Szkody, P. et al. 2002, AJ, 123, 430

- Tappert, C., Thorstensen, J. R., Fenton, W. H., Bennert, N., Schmidtbreick, L., & Bianchini, A. 2001, *A&A*, 380, 533
- Thorstensen, J. R., & Freed, I. W. 1985, *AJ*, 90, 2082
- Thorstensen, J. R. 1986, *AJ*, 91, 940
- Thorstensen, J. R., Patterson, J., Thomas, G., & Shambrook, A. 1996, *PASP*, 108, 73
- Thorstensen, J. R., Fenton, W. H., Patterson, J. O., Kemp, J., Krajci, T., & Baraffe, I. 2002, *ApJ*, 567, L49
- Thorstensen, J. R., Fenton, W. H., Patterson, J., Kemp, J., Halpern, J., & Baraffe, I. 2002, *PASP*, 114, 1117
- Tonry, J. & Davis, M. 1979, *AJ*, 84, 1511
- Warner, B. 1987, *MNRAS*, 227, 23
- Warner, B. 1995, *Cataclysmic Variables* (Cambridge University Press)

Table 1. Journal of Observations

Date [UT]	N	HA (start) [hh:mm]	HA (end) [hh:mm]
TT Crt:			
2000 Jan 6	2	+1 : 26	+1 : 32
2000 Apr 7	1	+1 : 53	...
2001 Dec 18	2	+0 : 04	+0 : 14
2001 Dec 25	3	-2 : 49	-2 : 28
2001 Dec 27	2	-2 : 27	-2 : 17
2002 Jan 19	3	-1 : 37	+2 : 25
2002 Jan 20	2	-0 : 20	+2 : 11
2002 Jan 21	4	-3 : 32	+1 : 48
2002 Jan 22	4	-3 : 01	+2 : 11
2002 Jan 24	3	-1 : 27	+1 : 23
2002 Feb 16	2	-0 : 18	-0 : 07
2002 Feb 20	1	+3 : 39	...
2002 Jun 12	1	+1 : 58	...
2002 Jun 13	1	+2 : 13	...
2002 Jun 14	1	+2 : 23	...
2002 Dec 13	1	-0 : 13	...
2003 Jun 20	1	+2 : 41	...
2003 Jun 21	1	+2 : 44	...
2003 Jun 22	1	+2 : 32	...
EZ Del:			
2002 Jun 14	13	-2 : 26	-0 : 29
2002 Jun 15	2	-2 : 11	-2 : 02
2002 Jun 16	5	-4 : 02	+0 : 50
2002 Jun 17	6	-3 : 21	+0 : 32
2003 Jun 23	6	-4 : 56	+1 : 17
2003 Jun 24	7	-4 : 27	-3 : 31
2003 Jun 25	9	+0 : 33	+1 : 38
LL Lyr:			
2000 Jul 5	3	+2 : 38	+4 : 06
2000 Jul 6	9	-2 : 34	-0 : 59
2000 Jul 7	2	-3 : 05	-2 : 55
2001 May 12	6	-0 : 05	+0 : 17

Table 1—Continued

Date [UT]	N	HA (start) [hh:mm]	HA (end) [hh:mm]
2001 May 14	18	–1 : 36	–0 : 35
2001 May 15	20	–2 : 55	+1 : 03
2001 May 16	12	–4 : 59	+0 : 47
2001 May 18	8	–4 : 33	–3 : 25
2001 Jun 26	1	+1 : 22	...
2001 Jun 27	6	–3 : 42	+3 : 23
2001 Jun 28	3	–3 : 48	–3 : 30
2001 Jun 29	3	–1 : 55	–1 : 38
2002 Jun 15	1	–1 : 14	...
2002 Jun 16	1	–2 : 41	...
2002 Oct 26	1	+2 : 20	...
2003 Jun 23	3	–1 : 29	–1 : 12
UY Pup:			
2002 Feb 20	2	+2 : 10	+2 : 22
2002 Feb 21	11	–2 : 26	+3 : 05
2002 Feb 22	7	–2 : 07	+2 : 16
2002 Oct 29	1	–1 : 32	...
2002 Oct 30	1	–0 : 09	...
2002 Oct 31	1	+0 : 02	...
2002 Nov 1	2	–1 : 14	–1 : 01
2002 Dec 12	4	–3 : 51	+2 : 33
2002 Dec 13	6	–3 : 30	+2 : 38
2002 Dec 14	1	–2 : 53	...
2002 Dec 16	3	–2 : 20	+1 : 07
2002 Dec 19	5	+0 : 19	+3 : 27
2003 Feb 1	1	–0 : 43	...
2003 Feb 2	1	+0 : 33	...
RY Ser:			
2003 Jun 20	4	+0 : 09	+3 : 42
2003 Jun 21	4	–2 : 44	+3 : 14
2003 Jun 22	3	–2 : 48	+3 : 00
2003 Jun 23	2	–2 : 18	–2 : 09
2003 Jun 25	1	–0 : 35	...
CH UMa:			

Table 1—Continued

Date [UT]	N	HA (start) [hh:mm]	HA (end) [hh:mm]
2000 Jan 10	1	+3 : 22	...
2002 Feb 16	1	–0 : 29	...
2002 Feb 17	2	+1 : 51	+2 : 04
2002 Feb 20	1	+4 : 43	...
2002 Feb 21	2	–3 : 20	+3 : 10
2002 Feb 22	5	–3 : 24	+5 : 13
2002 Jun 14	1	+3 : 34	...
2002 Jun 15	1	+3 : 40	...
2002 Jun 16	1	+3 : 36	...
2002 Jun 17	1	+3 : 45	...
2002 Oct 26	1	–2 : 21	...
2002 Oct 29	1	–2 : 18	...
2002 Dec 13	1	+0 : 32	...
2002 Dec 19	4	–1 : 27	+1 : 27
2003 Jan 31	1	+3 : 57	...
2003 Jun 20	2	+4 : 29	+5 : 06
2003 Jun 21	1	+4 : 00	...
2003 Jun 23	1	+3 : 56	...
SDSS 0813+45:			
2002 Jan 19	11	–4 : 15	+5 : 03
2002 Jan 20	5	–1 : 12	+3 : 39
2002 Jan 21	5	–2 : 42	+2 : 49
2002 Jan 22	3	–0 : 29	+3 : 39
2002 Jan 24	1	+1 : 38	...
2002 Feb 19	1	+0 : 46	...

Table 2. Emission Features

Feature	E.W. ^a (Å)	Flux ^b (10^{-16} erg cm ⁻² s ⁻¹)	FWHM ^c (Å)
TT Crt:			
H γ	14	176	32
H β	13	165	28
NaD	-3	-47	11
H α	17	237	29
EZ Del:			
H γ	18	87	16
HeI λ 4471	2	11	6
H β	22	82	14
HeI λ 4921	3	9	17
HeI λ 5015	3	10	16
Fe λ 5169	1	5	11
HeI λ 5876	5	14	13
NaD	-1	-2	9
H α	35	85	16
HeI λ 6678	3	8	16
HeI λ 7067	2	4	19
LL Lyr:			
H γ	38	137	21
HeI λ 4471	10	33	35
H β	58	147	26
HeI λ 4921	9	23	27
HeI λ 5015	12	30	42
Fe λ 5169	5	14	21
HeI λ 5876	16	37	29
H α	68	172	24
HeI λ 6678	8	18	31
UY Pup:			
H γ	8	191	12
HeI λ 4471	1	35	11
H β	10	249	12

Table 2—Continued

Feature	E.W. ^a (Å)	Flux ^b (10 ⁻¹⁶ erg cm ⁻² s ¹)	FWHM ^c (Å)
HeI λ4921	1	33	14
HeI λ5015	1	30	12
HeI λ5876	3	66	12
NaD	-1	-25	10
Hα	17	387	14
HeI λ6678	2	47	16
HeI λ7067	2	34	17
RY Ser:			
Hγ	26	198	20
HeI λ4471	6	53	11
HeII λ4686	3	23	16
Hβ	19	179	12
HeI λ4921	1	11	11
HeI λ5015	2	16	12
HeI λ5876	5	58	11
NaD	-2	-25	9
Hα	22	296	12
HeI λ6678	3	36	17
HeI λ7067	2	31	20
CH UMa:			
Hγ	31	798	12
HeI λ4471	13	314	14
Hβ	35	980	12
HeI λ4921	4	109	12
HeI λ5015	4	105	10
HeI λ5876	9	311	11
NaD	-3	-87	11
Hα	36	1268	11
HeI λ6678	5	168	15
HeI λ7067	3	113	16
SDSS 0813+45:			
Hγ	19	35	10
HeI λ4471	13	22	19

Table 2—Continued

Feature	E.W. ^a (Å)	Flux ^b (10 ⁻¹⁶ erg cm ⁻² s ⁻¹)	FWHM ^c (Å)
H β	35	57	12
HeI λ 4921	2	4	10
HeI λ 5015	3	4	9
HeI λ 5876	6	11	11
NaD	-3	-6	10
H α	30	55	11
HeI λ 6678	4	6	17
HeI λ 7067	3	5	17

^aEmission equivalent widths are counted as positive.

^bAbsolute line fluxes are uncertain by a factor of about 2, but relative fluxes of strong lines are estimated accurate to ~ 10 per cent.

^cFrom Gaussian fits.

Table 3. Radial Velocities

Time ^a	v_{abs} (km s ⁻¹)	σ (km s ⁻¹)	v_{emn} (km s ⁻¹)	σ (km s ⁻¹)
TT Crt:				
51550.0607	36	16	-75	21
51550.0648	-12	17	-71	26
51641.8325	44	15	-118	13
52262.0528	-203	14	74	23
52262.0599	-219	14	4	27
52268.9147	190	19	-177	20
52268.9218	181	18	-188	20
52268.9290	196	17	-210	20
52270.9242	-271	19	-2	27

^aHeliocentric Julian data of mid-exposure, minus 2 400 000.

Note. — Emission (H α) and absorption radial velocities. A sample is shown here; full version is available in the electronic version of the paper.

Table 4. Fits to Radial Velocities

Data set	T_0^a	P (d)	K (km s ⁻¹)	γ (km s ⁻¹)	N	σ^b (km s ⁻¹)
TT Crt (abs)	297.0254(9)	0.2683522(5)	212(5)	-23(3)	36	15
TT Crt (emn)	297.163(3)	...	124(8)	-77(6)	36	27
EZ Del (emn) ^c	442.917(2)	0.2234(5)	91(7)	-6(5)	48	21
LL Lyr (emn) ^c	042.079(3)	0.249069(4)	75(5)	-35(4)	97	17
UY Pup (abs)	577.183(3)	0.479269(7)	102(4)	45(3)	46	14
UY Pup (emn)	576.948(5)	...	96(5)	28(4)	49	18
RY Ser (abs)	812.788(3)	0.3009(4)	87(6)	-10(4)	14	12
RY Ser (emn)	812.639(6)	...	73(10)	-30(6)	14	20
CH UMa (abs)	442.787(3)	0.3431843(6)	76(3)	-15(2)	28	8
CH UMa (emn) ^c	442.616(9)	...	33(5)	-14(4)	28	13
SDSS0813 (abs)	296.080(5)	0.2890(4) ^d	54(7)	-29(4)	23	15
SDSS0813 (emn) ^c	295.942(6)	...	32(5)	-22(3)	26	11

Note. — Parameters of least-squares sinusoid fits to the radial velocities, of the form $v(t) = \gamma + K \sin(2\pi(t - T_0)/P)$. Where both emission and absorption velocities are available, the period quoted is the weighted average of the periods derived from separate fits to the two data sets, and the period is only given on the first line.

^aHeliocentric Julian Date minus 2452000. The epoch is chosen to be near the center of the time interval covered by the data, and within one cycle of an actual observation.

^bRoot-mean-square residual of the fit.

^cIn these cases the emission line velocities which were fitted were not derived using the double-gaussian convolution; in EZ Del and LL Lyr the lack of secondary-star velocities precluded checking the phase, and in RY Ser and CH UMa the lines were narrow enough that the double-gaussian method did not offer any advantage.

^dThere is slight ambiguity in the adopted period, see the discussion in the text.

Table 5. Inferences from Secondary Stars

Star	Type	Synthetic V (mag)	Assumed M_2^a M_\odot	Deduced R_2 R_\odot	M_V^b (mag)	A_V (mag)	Distance (pc)
TT Crt	K5 \pm 1	16.8 \pm 0.3	0.65 \pm 0.15	0.69 \pm 0.06	7.3 \pm 0.4	0.1	760(+200, –160)
EZ Del	M1.5 \pm 0.5	20.0 \pm 0.4	0.45 \pm 0.10	0.52 \pm 0.07	9.5 \pm 0.5	0.5 \pm 0.2	1000(+380, –280)
LL Lyr	M2.5 \pm 1.5	20.0 \pm 0.4 ^c	0.39 \pm 0.14	0.55 \pm 0.07	9.9 ^c	0.2	960(+420, –300)
UY Pup	K4 \pm 2	17.3 \pm 0.5	0.65 \pm 0.25	1.0 \pm 0.2	6.3 \pm 0.8	0.5	1300 (+600, –500)
RY Ser	K5 \pm 1	17.4 \pm 0.3	0.6 \pm 0.1	0.74 \pm 0.05	7.2 \pm 0.4	1.2 \pm 0.3	620(+240, –170)
CH UMa	K5.5 \pm 1	15.9 \pm 0.4	0.6 \pm 0.15	0.78 \pm 0.08	7.3 \pm 0.6	0.18	480(+180, –130)
SDSS0813+45	K5.5 \pm 1	19.1 \pm 0.4	0.63 \pm 0.10	0.72 \pm 0.04	7.4 \pm 0.3	0.15	2100 \pm 500

^aNote carefully that these masses are not measured, but are estimates guided by the models of Baraffe & Kolb (2000). They are used *only* to constrain R_2 , which depends only on the cube root of M_2 , so this does not contribute substantially to the error budget.

^bAbsolute visual magnitude inferred for the secondary alone, on the basis of surface brightness and Roche lobe size (see text).

^cThe error estimate for LL Lyr is complicated because the secondary flux is correlated with the spectral type. Fortunately, these errors tend to compensate in the distance calculation, because a later-type star, with stronger features, is inferred to contribute less to the summed spectrum, but is also inferred to be intrinsically fainter. The final distance uncertainties include this effect.

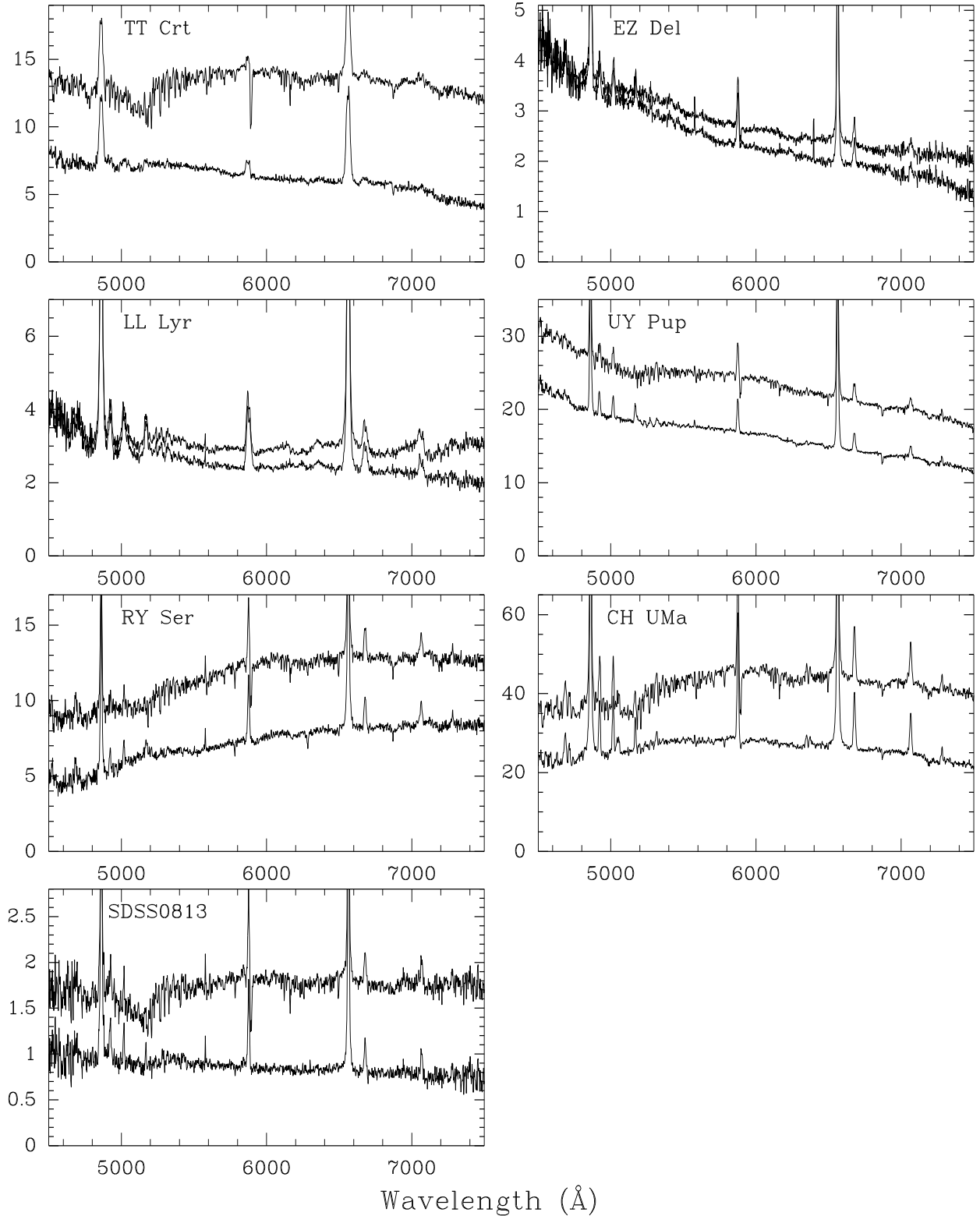


Fig. 1.— A montage of spectra. The vertical scale in each plot is in units of $10^{-16} \text{ erg s}^{-1} \text{ cm}^{-2} \text{ \AA}^{-1}$, subject to calibration uncertainties of some tens of percent. The lower trace in each panel shows the data after a scaled late-type star has been subtracted away (see text and Table 5). In all cases except EZ Del and LL Lyr the original spectra were shifted into the rest frame of the secondary star before averaging.

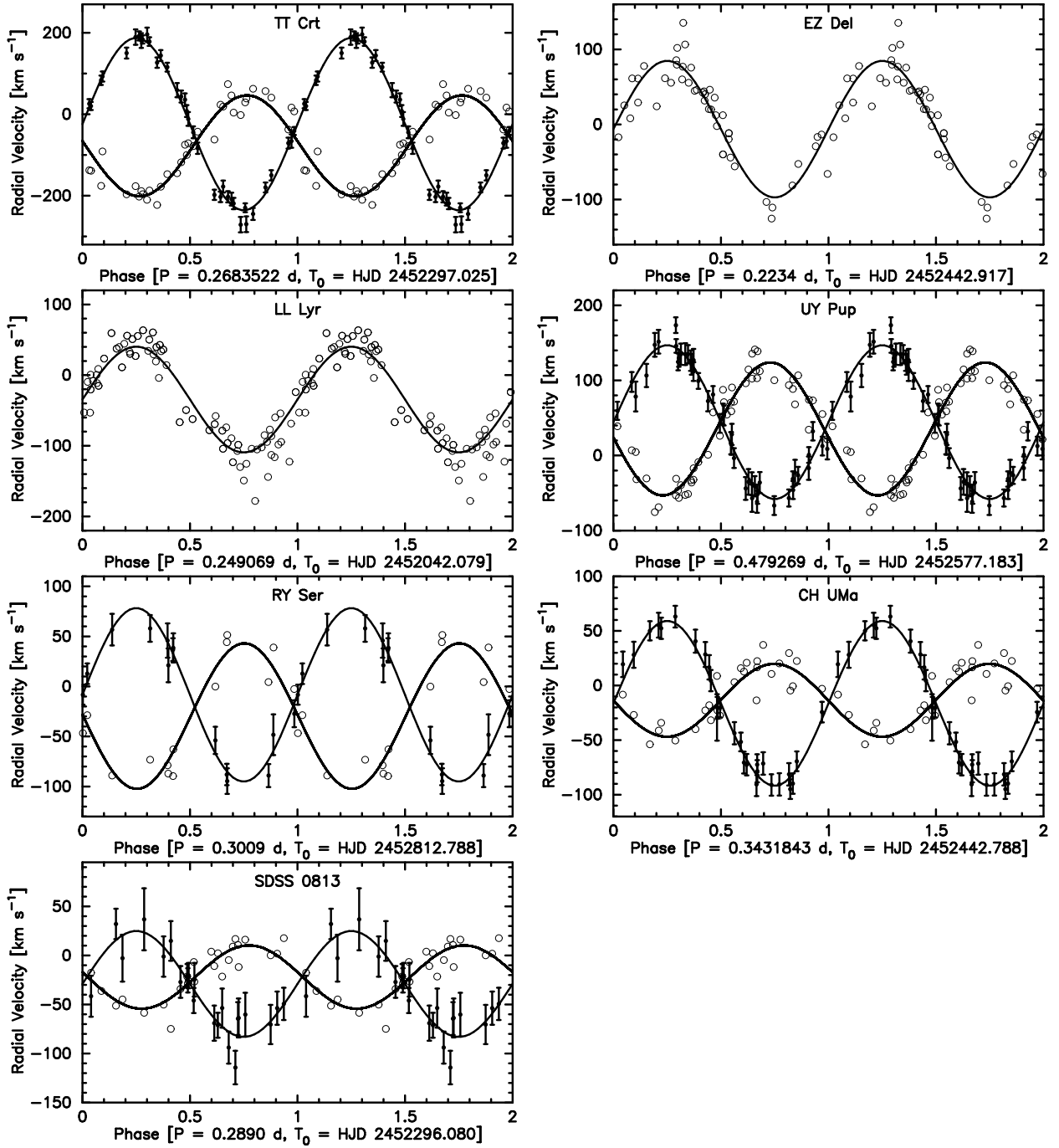


Fig. 2.— Absorption (solid dots with error bars) and emission (open circles) radial velocities folded on the adopted orbital periods. Best-fit sinusoids are superposed. All data are shown twice for continuity.